

A data-driven Vertical Stabilization system for the ITER tokamak based on Dynamic Mode Decomposition

Luigi Emanuel di Grazia^a, Massimiliano Mattei^{b,c}, Adriano Mele^d, Alfredo Pironti^{b,c}

^a*Dipartimento di Ingegneria, Università degli Studi della Campania Vanvitelli, Via Roma 29, Aversa, 81031, CE, Italy*

^b*Consorzio CREATE, via Claudio 21, Napoli, 80125, NA, Italy*

^c*Dipartimento di Ingegneria Elettrica e Tecnologie dell'Informazione, Università degli Studi di Napoli Federico II, via Claudio 21, Napoli, 80125, state{NA} Italy*

^d*Dipartimento di Economia, Ingegneria, Società e Impresa, Università degli Studi della Tuscia, Largo dell'Università - Campus Riello, blocco F, Viterbo, 01100, VT, Italy*

Abstract

In this article, we propose an online method to estimate an approximate linear model of a vertically unstable tokamak plasma to consequently adapt the parameters of a Vertical Stabilization controller. The identification procedure is based on the Dynamic Mode Decomposition with control approach, while the tuning procedure takes advantage of linear control theory to impose the desired crossing frequency and gain margins. The proposed technique is aimed at controlling ITER elongated plasmas using the VS3 stabilization coils, located inside the vessel. The effectiveness of the method is proven by means of numerical simulations carried out with the CREATE-NL+ free boundary evolutionary code, also considering the presence of realistic measurement noise levels.

Keywords:

tokamaks, magnetic control, vertical stabilization, dynamic mode decomposition, online identification, data-driven control

1. Introduction

Tokamaks [1] are regarded as the most promising concept for a viable commercial nuclear fusion energy reactor. They are complex devices where a ring of plasma is heated up to $\sim 10^8$ degrees and confined by means of powerful magnetic fields. The operation of these machines calls for the solution of a number of different control problems, among which *magnetic* control [2, 3] plays a fundamental role. In particular, the magnetic control system is in charge of regulating the currents that flow in the conducting coils in order to achieve a desired magnetic field configuration. This configuration is indirectly specified in terms of controlled quantities of interest, such as the total plasma current, the position of the plasma centroid and of magnetic field

null point(s), or plasma-wall gaps. However, the most fundamental task fulfilled by a magnetic control system is perhaps that of stabilizing elongated plasma configurations: while such configurations are efficient from the point of view of fusion power generation, they are known to be intrinsically unstable [1, §6.15], [4, 5].

Several approaches are described in the scientific literature to solve the Vertical Stabilization (VS) problem, most of which are model-based. Often, the VS controller is specifically designed for a given plasma scenario, as in the case of the JET [6] or DIII-D [7]. Similarly, a model-based VS algorithm has also been proposed for the forthcoming ITER tokamak [8, 9]; this algorithm has been experimentally tested on the EAST device, which has a similar superconducting coils layout [10]. Other approaches include nonlinear adaptive control [11] and MPC [12].

One of the main parameters influencing the design of a VS control system is the plasma *growth rate* γ , defined as the (real) unstable eigenvalue of

Email addresses:

luigiemanuel.digrazia@unicampania.it (Luigi Emanuel di Grazia), massimiliano.mattei@unina.it (Massimiliano Mattei), adriano.mele@unitus.it (Adriano Mele), pironti@unina.it (Alfredo Pironti)

the plasma linearized response model in the neighborhood of the considered operational configuration, which is associated to the coherent, unstable motion of the plasma in the vertical direction. The real-time reconstruction of this parameter could provide valuable information for adaptive VS control algorithms. However, since the VS control loop usually needs to operate with a very low latency time, computing a full linearized plasma model at each controller time step would be impractical in a real-time scenario, even though some recent attempt in this direction has been made by leveraging the computing power of GPUs [13].

The main disadvantage of standard, model-based VS design approaches is that, at least in principle, a dedicated controller must be tuned for each plasma configuration of interest, usually based on a linearized plasma response model computed offline. This also means that, if different plasma configurations are foreseen during a scenario, different controllers must be designed and validated offline, and their use must be scheduled in advance according to the foreseen discharge evolution. In this view, an adaptive VS algorithm would increase the flexibility of the magnetic control system, reducing the deployment time due to offline design and validation. An attempt in this direction has been made with an alternative approach for the VS based on Extremum Seeking algorithm [14, 15]. This solution, however, still requires the design of an observer, based on a reduced order plasma linearized model, to estimate the plasma motion along the unstable eigenvector.

A possibility to avoid control solutions based on pre-existing models could be to resort to online model identification procedures based on measurements. In this work, we make use of an identification technique based on the Dynamic Mode Decomposition with control (DMDc) approach [16], which extends the Dynamic Mode Decomposition (DMD) to the case of (linear) systems with control. A comprehensive overview on DMD and its applications can be found in [17]. DMD was originally introduced in the fluid dynamics community [18, 19] as a tool to identify coherent spatio-temporal structures in a flow, together with the associated growth rates and oscillation frequencies, based on measured data. The DMD algorithm can be easily derived for linear systems (as briefly discussed for the sake of self-containedness in sec. 3), but is often used for nonlinear systems as well, thanks to its connections with the Koopman operator theory [20], [17, §1.2]. Applications of the DMD algorithm to the

field of plasma physics and nuclear fusion can be found in [21, 22, 23].

The rest of the paper is structured as follows. In sec. 2 some tools for electromagnetic modelling used in the rest of the paper are introduced. A simplified rigid filamentary model of the vertical instability is briefly discussed as a motivation for the proposed online identification procedure, and some information on the current proposal for the ITER VS system is given. In sec. 3, a model identification technique based on DMD is described, and a comparison between the (reduced-order) identified models and the corresponding full linearized models obtained through the linearization of the plasma equilibrium equations (by means of the CREATE-L code) is presented, showing the effectiveness of the procedure. Sec. 4 discusses a procedure to tune the VS controller based on the identified model. In sec. 5, numerical nonlinear simulations carried out with the CREATE-NL+ code are used to prove the validity of the overall control approach. Finally, some concluding remarks are provided in sec. 6.

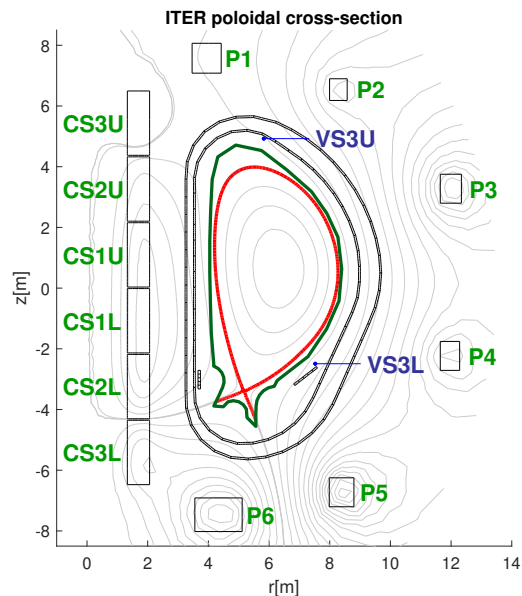


Figure 1: Poloidal cross-section of an elongated ITER tokamak plasma as obtained by means of the CREATE-NL+ code; the plasma boundary is shown in red, while a few isoflux curves are shown in gray. The superconductive PF coils are labeled in green, while the in-vessel coils $VS3U - VS3L$ (connected in anti-series to form the $VS3$ circuit) are indicated in blue. The First Wall is highlighted in dark green.

2. Preliminaries

2.1. Plasma modelling in axisymmetric geometry

In axi-symmetric conditions, the ideal MHD equilibrium of a tokamak plasma can be described by using cylindrical coordinates (r, z) in terms of the poloidal flux per radian function $\psi = \psi(r, z)$, defined as the magnetic flux per radian across a disk at height z , with radius r and with axis $r = 0$. The ψ distribution in the tokamak vacuum chamber can be found as the solution of a 2D elliptic partial differential equation (PDE) known as the Grad-Shafranov equation

$$\Delta^* \psi(r, z) = -\mu_0 r j_\phi(r, z), \quad (1)$$

where μ_0 is the vacuum magnetic permeability and Δ^* is a differential operator defined as

$$\Delta^* = r \frac{\partial}{\partial r} \left(\frac{1}{r} \frac{\partial \psi}{\partial r} \right) + \frac{\partial}{\partial z} \left(\frac{\partial \psi}{\partial z} \right). \quad (2)$$

The source term j_ϕ represents the toroidal current density, which in the plasma region is assumed to be

$$j_\phi = \frac{f}{\mu_0 r} \frac{df}{d\psi} + r \frac{dp}{d\psi} \quad (3)$$

where p is the total plasma pressure and $f := rB_\phi$ is the so-called poloidal current function, B_ϕ being the toroidal magnetic field.

Equation 1 also holds in the conductor cross-section, where the toroidal current density is known ($j_\phi = j_{ext}$) and in vacuum, where $j_\phi = 0$. The following boundary conditions are assigned

$$\psi(0, z) = 0 \quad (4a)$$

$$\lim_{(r^2+z^2) \rightarrow \infty} \psi(r, z) = 0 \quad (4b)$$

It is a standard assumption that, inside the plasma region, p and f are themselves functions of the poloidal flux ψ , i.e. they are assumed constant on isoflux surfaces. This means that the source term $j_\phi(r, z)$ is a function of $\psi(r, z)$. The plasma current is usually constrained to flow inside the so-called plasma boundary, defined as the outermost closed isoflux line inside the vacuum chamber. This makes eq. (1) a free-boundary, nonlinear problem, which is usually solved by means of dedicated numerical procedures.

Eq. (1) can be coupled with the circuit equations describing the time evolution of the currents in the

active coils, in the passive structures and in the plasma itself

$$\dot{\Psi} + RI = V, \quad (5)$$

where Ψ is the vector of poloidal magnetic fluxes linked with circuits, R is the resistance matrix, I is the vector of currents in circuits, V contains the applied voltages (which are nonzero only for the active coils). Note that the term $\dot{\Psi}$ also takes into account the flux contribution coming from the plasma, which depends on the solution of (1) as the plasma is assumed to evolve through a series of MHD equilibrium states. On the other hand, the source terms in eq. (1) depend on the currents at the considered time instant. In practice, the evolutive problem coming from the coupling of GS equation (1) with the circuit dynamics (5) is solved by means of numerical solvers, such as the Finite Elements Method (FEM) code CREATE-NL+ [24] used for the simulations presented in sec. 5.

In order to design plasma magnetic controllers, the plasma response is often linearized in the neighborhood of the considered plasma equilibrium configuration. This can be done, for example, by means of the procedure implemented in the CREATE-L code [25], which has been used for the analysis of the method proposed in this article. The linearized response models obtained through CREATE-L have the form

$$L^* \delta \dot{I} + R \delta I = \delta V + L_E \delta \dot{w} \quad (6a)$$

$$\delta y = C \delta I + F \delta w \quad (6b)$$

where the vector δV contains the applied voltage, δI contains the current variations with respect to the equilibrium values L^* is the inductance matrix¹, δw contains the variations of input variables related to the current density distribution inside the plasma (usually parameterized in terms of poloidal beta β_p and internal inductance l_i), whose variation has an impact on the flux linked with circuits through the L_E matrix. The vector δy contains variations with respect to the equilibrium values of some outputs of interest, such as magnetic measurements, plasma-wall gaps, centroid and X-point positions; these variations are linked to the currents through the output matrix C , and to the plasma parameters through the matrix F . The linear system (6) can

¹The * apex indicates that this matrix is modified by the presence of the plasma; see also the discussion in the next section.

be recast in state-space form as

$$\begin{aligned}\delta\dot{x} &= A\delta x + B\delta u + E\delta\dot{w} \\ \delta\dot{y} &= C\delta x + F\delta w\end{aligned}\quad (7)$$

where $x = I$, $u = V$, $A = -L^{*-1}R$, $B = L^{*-1}$ and $E = L^{*-1}L_E$.

2.2. Vertical instability and rigid displacement model

It is a well-known fact that elongated plasma configurations in tokamaks are vertically unstable [1, §6.15]. It is possible to draw some conclusions on such instability even by making use of a very crude filamentary model of the plasma. In the simplest possible model of this unstable vertical motion, the plasma ring is approximated by a rigid filament carrying a current I_p , which is allowed to move in the vertical direction only. We denote the radius of this filament by r_p and its vertical position by z_p . The vertical force exerted on this filament by a (radial) magnetic field can be expressed as

$$m_p\ddot{z}_p = -2\pi r_p I_p B_r(z_p, I_a, I_e) \quad (8)$$

where m_p is the plasma mass and B_r is the radial magnetic field component at (r_p, z_p) , which depends on the filament vertical position z_p and on the currents in the active and passive circuits, I_a, I_e respectively. Elongated plasma configurations are obtained by applying a quadrupole magnetic field [4], which means that the radial field has a nonzero downward gradient along the vertical direction, as shown in fig. 2. As it can be seen, the radial field is larger far from the equilibrium position, which means that a small displacement of the plasma results in a net force which pushes the plasma ring further away from the equilibrium, resulting in a positive-feedback mechanism which makes the equilibrium position (i.e. the point where $B_r = 0$) unstable.

Eq. (8) can be coupled with the circuit dynamics (5) as follows

$$\begin{aligned}L_a\dot{I}_a + R_a I_a + M_{ae}\dot{I}_e + \dot{\psi}_{ap}(z_p) &= V_a \\ L_e\dot{I}_e + R_e I_e + M_{ea}\dot{I}_a + \dot{\psi}_{ep}(z_p) &= 0\end{aligned}\quad (9)$$

where the pedices (a, e) refer to active and passive currents respectively, R, L, M represent resistance, self-inductance and mutual inductance matrices and $\psi_{(a,e)p}$ is the flux contribution generated by the plasma current distribution and enclosed by

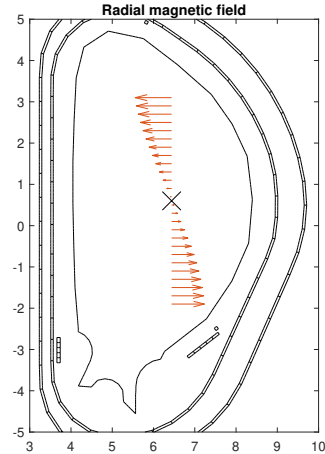


Figure 2: Radial magnetic field component for the elongated plasma cross-section shown in fig. 1 along a vertical line passing through the magnetic axis (indicated by the black cross).

the active and passive elements respectively. The flux terms $\psi_{(a,e)p}(z_p)$ are linked to the radial fields $B_r^{(a,e)}(z_p)$, generated by the active and passive currents respectively, through the relation

$$B_r^{(a,e)} = -\frac{1}{2\pi r_p} \frac{\partial \psi_{p(a,e)}}{\partial z_p} \quad (10)$$

By linearizing the expression of $B_r(z_p, I_a, I_e)$ and neglecting the plasma mass m_p in eq. (8), a static relation between z_p and the currents $I_{(a,e)}$ can be obtained (the details are omitted here for the sake of brevity). This allows to derive a linear relation between the terms $\psi_{(a,e)p}(z_p)$ and the variations of the considered currents $\delta I_{(a,e)}$, leading to the (linearized) circuit model

$$\begin{bmatrix} \delta\dot{I}_a \\ \delta\dot{I}_e \end{bmatrix} = -L^{*-1}R \begin{bmatrix} \delta I_a \\ \delta I_e \end{bmatrix} + L^{*-1} \begin{bmatrix} \delta V_a \\ 0 \end{bmatrix} \quad (11)$$

where L^* is a modified inductance matrix, that takes into account both the destabilizing force generated by a vertical motion of the plasma and the stabilizing effect of the passive structures (see also eq. (6a) - we used again the same symbol L^* , with a slight abuse of notation, to underline that this inductance matrix is not the geometric coil inductance, but also takes into account the presence of the plasma). From eq. 11 it appears clearly that the characteristic time constant of the vertical instability depends on the time constant of the passive structures surrounding the plasma through the term $-L^{*-1}R$. In practice,

the resulting growth rate is usually in the order of $10^1 \sim 10^3 \text{ s}^{-1}$.

2.3. Vertical Stabilization system

The VS system proposed for ITER relies on coils that are placed both outside and inside the tokamak vessel. However, among the available actuators the so called *VS3U* – *VS3L* in-vessel coils are much more effective as they suffer less from the shielding of the passive conductive structures, they are closer to the plasma and they are more reactive to voltage commands due to their lower inductance. On the other hand, they are adequate to quickly react to variations in the plasma vertical speed, but not to position displacements, since they are not designed to carry high currents for a long time. In this view, the considered VS control loop exploits *VS3U* – *VS3L* to keep the plasma vertical velocity close to zero, while the task of regulating the position of the plasma centroid is demanded to another, dedicated control loop, which relies on the out-vessel coils.

The VS3 coils are connected in anti-series in order to produce an approximately radial field inside the vacuum chamber and thus serve as a suitable actuator for the vertical stabilization system. We denote the current flowing in the resulting circuit as I_{VS3} and consider the following control law from [8]

$$u = K_2 \dot{z}_p + K_I I_{VS3} \quad (12)$$

u being VS3 voltage and z_p the vertical position of the plasma centroid.

This kind of control law has been experimentally validated on the EAST tokamak [10, 26], where an additional lead network was added and both the control gains, and the network parameters were optimized in order to improve the resulting stability margins [27]. Note that in tokamaks an estimate of the vertical position z_p of the plasma is usually obtained as a linear combination of magnetic measurements. Then, the vertical velocity \dot{z}_p is obtained from the estimated z_p through a numerical derivative. In our analysis, we will use the following derivative filter

$$F(s) = \frac{s}{1 + 10^{-3}s}. \quad (13)$$

Moreover, in what follows we will also consider a simplified model of the power supplies having the following transfer function

$$W_{ps}(s) = \frac{e^{-s\tau_1}}{1 + s\tau_2} \quad (14)$$

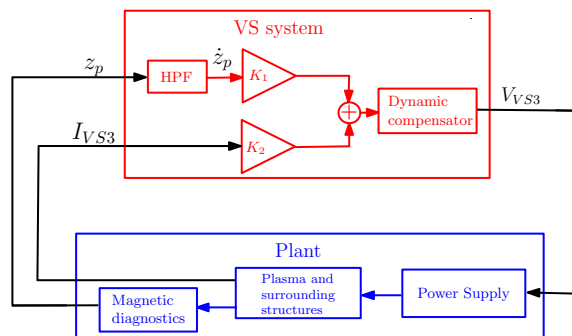


Figure 3: Schematic of the considered VS system.

with $\tau_1 = 2.5 \text{ ms}$ and $\tau_2 = 7.5 \text{ ms}$ [28].

Starting from these considerations, a schematic view of the VS system considered in the rest of this article is shown in fig. 3. In the proposed architecture a dynamic compensator is included in the VS system, similarly to what has been done for the EAST tokamak [10]. However, while a lead network was used in the EAST case in order to increase the resulting phase margin, for ITER a lag network is added to assign the crossing frequency of the loop function in the controller tuning procedure discussed in sec. 4. Intuitively, this can be justified by taking into account the fact that the typical growth rates associated to ITER plasmas are much smaller than the ones obtained in EAST, so there is less need to anticipate the controller action; on the other hand, it is important to limit the bandwidth to avoid stressing the power supplies, which are slower in the ITER case.

3. Model identification

As discussed in sec. 2.2, a very simple filamentary model of the plasma is already capable of capturing the vertical instability of the system. However, rigid displacement models cannot be used for radial position and/or shape control, since they cannot describe radial displacements of the plasma or boundary deformations. Moreover, in the case of highly shaped plasmas, filamentary models derived from first principles can provide an inaccurate estimate of the plasma growth rate, and hence of the unstable dynamics [29]. For these reasons, when designing model-based controllers, usually more sophisticated approaches are preferred, such as perturbed equilibrium/nonrigid displacement ones [29, 30, 31].

On the other hand, linearized models can be costly to compute, and hence they are not suitable as a ba-

sis for real-time adaptive control algorithms. Moreover, a VS system in the form (12) only requires the knowledge of the dynamics relating the voltage on the stabilization circuit V_{VS3} to the current I_{VS3} and z_p , and hence to design such a controller a simplified model is often sufficient. For this reason, we propose to resort to a simple 2^{nd} order model whose structure is inspired by (11). In order to obtain good prediction and modeling accuracy, the parameters are identified online on the basis of experimental measurements.

In this section, we will give some details on the considered simplified model structure (sec. 3.1) and on the identification procedure (sec. 3.2); then, an example of an identified linear model is provided in sec. 3.3, and is further refined in sec. 3.4. A possible automated controller synthesis procedure is discussed in sec. 4.

3.1. Model structure

The simplest linear model to catch the I_{VS3} dynamics and its relation to z_p takes into account the stabilization circuit only

$$L_{VS3} \delta \dot{I}_{VS3} + R_{VS3} \delta I_{VS3} + a \delta z_p = \delta V_{VS3} \quad (15)$$

where the term $a\delta z_p$ represents the voltage induced in the VS3 by the vertical plasma movement. Eq. (15) is coupled with the following scalar vertical instability model [5]

$$\delta \dot{z}_p = \gamma \delta z_p + d \delta V_{VS3} \quad (16)$$

In this model, the vertical motion is characterized by the single unstable eigenvalue γ (the plasma growth rate) and is affected by the voltage applied to the active control circuit V_{VS3} through a scalar coefficient d . In this simplified view, the effect of the other control circuits, which are placed outside the vessel and act on slower time scales, is regarded as a slowly varying disturbance.

It is worth to remark that the identified values of L_{VS3} and R_{VS3} will in general be close – but different from – the actual parameters of the VS3 circuit. In particular, the simplified model inductance will be affected by the dynamics of both the induced passive currents and the plasma, while the identified resistance may suffer from a bad identification of the steady-state behaviour of the system. For this reason, while a deviation from the actual inductance value of the VS3 circuit is necessary for the identified model to closely describe the real-world plasma

dynamics, deviations in the value of R_{VS3} will in general be regarded as identification errors and corrected through the dedicated procedure described in sec. 3.4.

In addition to that, we also allow δz_p in eq. (16) to directly depend on δI_{VS3} , and hence rewrite (16) as

$$\delta \dot{z}_p = b \delta I_{VS3} + c \delta z_p + d \delta V_{VS3} \quad (17)$$

This provides an additional degree of freedom to the identification procedure, although the identified value of b is expected to be relatively small. Notice that, since the term $c \delta z_p$ represents the unstable contribution to the plasma motion due to the B_r vertical gradient (see fig. 2), we expect $c > 0$.

By substituting eq. (17) in eq. (15) we obtain the following reduced model structure

$$\begin{aligned} \begin{bmatrix} \delta \dot{I}_{VS3} \\ \delta \dot{z}_p \end{bmatrix} &= \begin{bmatrix} -\frac{(R_{VS3}+ab)}{L_{VS3}} & -\frac{ac}{L_{VS3}} \\ b & c \end{bmatrix} \begin{bmatrix} \delta I_{VS3} \\ \delta z_p \end{bmatrix} \\ &+ \begin{bmatrix} \frac{(1-ad)}{L_{VS3}} \\ d \end{bmatrix} \delta V_{VS3} \\ &= \begin{bmatrix} a_{11} & a_{12} \\ a_{21} & a_{22} \end{bmatrix} \begin{bmatrix} \delta I_{VS3} \\ \delta z_p \end{bmatrix} + \begin{bmatrix} b_1 \\ b_2 \end{bmatrix} \delta V_{VS3}, \end{aligned} \quad (18)$$

The matrix transfer function at $s = 0$ is given by

$$H(0) = - \begin{bmatrix} a_{11} & a_{12} \\ a_{21} & a_{22} \end{bmatrix}^{-1} \begin{bmatrix} b_1 \\ b_2 \end{bmatrix}.$$

With a slight abuse of notation (since system (18) is unstable), we will refer to the elements of $H(0)$ as static gains.

3.2. Identification procedure

To obtain an identified model for the design of the VS controller, we make use of the DMDc approach [16]. To start with, we consider the discrete-time version of (18)

$$x(k+1) = Ax(k) + Bu(k) \quad (19)$$

where $x(k) = [\delta I_{VS3}(k) \ \delta z_p(k)]^T$ and $u(k) = \delta V_{VS3}(k)$. By defining the following matrices

$$X_{0,T} = [x(0) \ x(1) \ \dots \ x(T-1)] \quad (20a)$$

$$X_{1,T+1} = [x(1) \ x(2) \ \dots \ x(T)] \quad (20b)$$

$$U_{0,T} = [u(0) \ u(1) \ \dots \ u(T-1)] \quad (20c)$$

model (19) can be rewritten as

$$X_{1,T+1} = AX_{0,T} + BU_{0,T} = [A \ B] \begin{bmatrix} X_{0,T} \\ U_{0,T} \end{bmatrix}. \quad (21)$$

The identified model matrices \hat{A}, \hat{B} can then be obtained as

$$\begin{bmatrix} \hat{A} & \hat{B} \end{bmatrix} = X_{1,T+1} \begin{bmatrix} X_{0,T} \\ U_{0,T} \end{bmatrix}^\dagger, \quad (22)$$

where the superscript \dagger denotes the right pseudo-inverse.

Notice that, for the identification procedure to be effective, if $x \in \mathbb{R}^n, u \in \mathbb{R}^m$ the control input must be persistently exciting of order $n+1$, which in turn implies that the signals used for the identification must contain at least $(m+1)n+m$ samples (see [32, eq. (6)]). For the reduced model (18), $n=2, m=1$, and hence $T \geq 5$. In practice we found that a few hundred samples are required to obtain an accurate model. Interestingly, this is consistent with the dimension of a typical full size model (7).

To trigger the unstable mode, a train of VS3 voltage doublets is used. These voltage kicks are chosen to minimize their effect on the scenario, and in particular

- the impulses have a limited amplitude (50V for ITER);
- the duty cycle is 15%;
- the doublet directions are swapped to minimize potential drift effects during plasma discharges.

Note that the VS controller remains active during the kicks. This kind of perturbation is not new in the nuclear fusion literature, and the applied voltage impulses are not expected to represent a threat to plasma operation in an actual tokamak discharge. In fact, perturbations of the radial magnetic field produced by the VS system have also been proved to be beneficial as a possible tool for ELM pacing at JET [33].

After each kick, the data samples are collected and the identification process (22) is run. Then, the obtained model is used to tune the VS system, as discussed in sec. 4. In the simulations presented in this article, a time interval of 0.25 s, starting from the beginning of the kick, has been used for the identification; this choice corresponds to 500 samples at the considered sampling time of 0.5 ms.

Before concluding this section, it should be observed that, with respect to the more sophisticated model (7), in this identification procedure we are neglecting the effect of variations in the plasma internal current distribution (synthetically described by the term δw in (7)). These variations, however,

could have a significant impact on the estimated dynamics, and in principle should be explicitly taken into account. This is especially true in some specific situations, for example during the so-called LH or HL transitions; as a consequence, the identification procedure should be run far from such transients. For simplicity, in our analysis we neglect the effect of the δw term in (7) and assume that, during the time interval considered for the identification procedure, the plasma internal profiles remain approximately constant. Similarly, we assume that the plasma shape variations occur on a time scale that is significantly slower than the typical time constants of the VS system. This is usually a well-satisfied approximation in tokamak discharges, especially if control coils are superconducting and external to the vacuum vessel, and allows to neglect the variations in the active currents other than the VS one.

3.3. Identification example

To validate the proposed identification procedure, we considered a simulated plasma scenario segment that reproduces the first ~ 6 s of the ramp-down of one of the foreseen ITER scenarios. The plasma current is reduced from 9MA to 8.5MA (see fig. 5), while the plasma profile parameters β_p, l_i are kept constant through the simulation. To excite the unstable dynamics for the identification, a sequence of voltage kicks is applied to the in-vessel circuit, as shown in fig. 4. The model identification procedure runs every second, with the first voltage kick at $t = 0.15$ s. The time step of the simulation is fixed to 0.5ms, and 500 steps are used in the identification procedure, resulting in a time window of 0.25s.

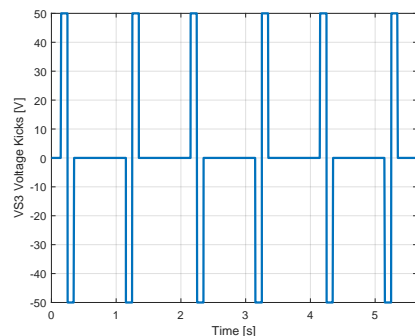


Figure 4: VS3 voltage kicks used for identification.

Fig. 6 shows a comparison between the identified growth rates and the eigenvalues of the linearized models obtained at the corresponding time instants

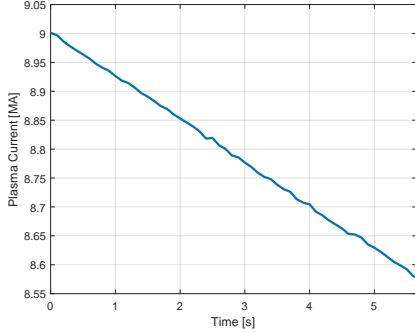


Figure 5: Plasma current evolution.

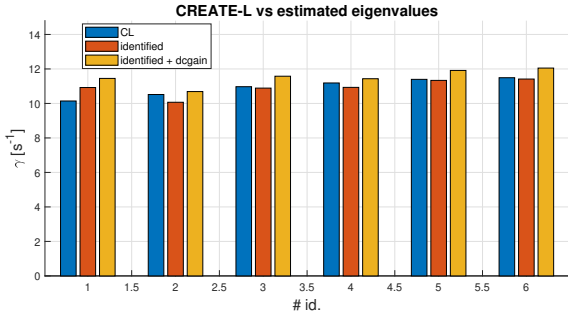


Figure 6: Growth rate comparison between CREATE-L (blue), identified models (red) and models identified by also fitting the static gain of the I_{VS3} channel with a weight $\alpha = 400$ (yellow). It can be noted that the proposed static gain adjustment leads to slightly higher estimates of the growth rate; this is not a problem, as in this case a higher value of γ represents a pessimistic scenario.

with CREATE-L (with state dimension $n = 123$, including active and plasma currents and equivalent axisymmetric passive currents). As it can be seen, the actual and identified growth rates show a satisfactory degree of accuracy.

As an example to verify the outcome of the identification procedure, we consider the identified linear models at $t = 2.4$ s and the corresponding linearized model obtained with CREATE-L. Fig. 7 shows a comparison between the Bode diagrams of these two models (dash-dotted red and solid blue, respectively). As it can be seen from the figure, the diagrams are reasonably similar, despite the significant reduction in the number of considered states. The identified model matrices, for the considered exam-

ple, are

$$\hat{A} = \begin{bmatrix} -19.73 & -2.627 \cdot 10^5 \\ 3.454 \cdot 10^{-5} & 11.38 \end{bmatrix} \hat{B} = \begin{bmatrix} 1147 \\ 1.435 \cdot 10^{-3} \end{bmatrix}. \quad (23)$$

It can be observed that, as expected, $b \approx 0$ and $c > 0$; in particular, c is very close to the unstable eigenvalue, which in this case is $\gamma = 11.08 \text{ s}^{-1}$. Moreover, from eq. (18) we can compute the identified inductance and resistance terms as

$$\hat{L}_{VS3} = \left(b_1 - \frac{a_{12}b_2}{a_{22}} \right)^{-1}$$

$$\hat{R}_{VS3} = \left(-a_{11} + \frac{a_{12}a_{21}}{a_{22}} \right) \hat{L}_{VS3}$$

The estimates obtained in this way are $\hat{R}_{VS3} = 0.016 \text{ } \Omega$, $\hat{L}_{VS3} = 0.85 \cdot 10^{-3} \text{ H}$ which are reasonably close to the actual values of $R_{VS3} = 0.012 \text{ } \Omega$, $L_{VS3} = 1 \cdot 10^{-3} \text{ H}$ used in CREATE-L. As it was already pointed out, note that we expect \hat{L}_{VS3} to be related to, but different from, its "true" value, as it is affected by the non-rigid behaviour of the plasma and by the presence of the passive structures, which are not explicitly taken into account in the structure of the identified model. On the other hand, the error in the estimation of the $VS3$ circuit resistance causes an error in the estimation of the transfer function from δV_{VS3} to δI_{VS3} in the low frequency region. This problem is discussed in the next section (see fig. 7).

3.4. Fitting procedure for the static gain

From fig. 7 it can be noticed that the static gain of the system is not perfectly identified. A possible explanation is that the data points used in the identification are sampled while the system is still evolving through a transient phase. However, we can exploit the physical knowledge of the plant to mitigate this phenomenon. In particular, from equation (15) it is possible to see that the static gain for the I_{VS3} channel is given by $1/R_{VS3}$, where the value of the $VS3$ circuit resistance R_{VS3} is usually known and/or can be accurately calibrated. On the other hand, we have no *a priori* knowledge of the static gain of the z_p transfer function.

For discrete-time systems, the static gain can be computed as

$$G_0 = (\mathbb{I} - A)^{-1}B, \quad (24)$$

where \mathbb{I} represents the identity matrix. We can then modify the DMDc algorithm in order to include

this information in the pseudo-inversion in eq. (22). To do so, first of all observe that eq. (24) can be rewritten as

$$G_0 = AG_0 + B. \quad (25)$$

Note that, for stable systems, this is equivalent to considering a fictitious data sample $x(k+1) = x(k) = G_0$ taken when the system has reached a regime condition under a unitary input. Since (25) has the same form of eq. (19), if an estimate of the static gain G_0 is available, we can include it in the identification procedure by modifying eq.(22) as follows

$$\begin{bmatrix} \hat{A} & \hat{B} \end{bmatrix} = [X_{1,T+1} \quad \alpha G_0] \begin{bmatrix} X_{0,T} & \alpha G_0 \\ U_{0,T} & 1 \end{bmatrix}^\dagger, \quad (26)$$

where α is a free scalar parameter that can be used to opportunely weigh the static gain condition. In practice, since an accurate measurement of the R_{VS3} parameter is usually available, we can force the first element in G_0 to be equal to $1/R_{VS3}$. On the other hand, since the gain on z_p is not known *a priori*, one possibility to obtain a value for the second entry in G_0 is to run the identification procedure in its plain form (22) first, then compute the estimated static gain \hat{G}_0 from \hat{A}, \hat{B} according to eq. (24), and set the second element in G_0 equal to the corresponding entry in \hat{G}_0 . This is equivalent to assuming that the first-guess of the parameter, obtained through the first identification procedure, is sufficiently reliable. As it can be seen from fig. 7, this procedure allows to obtain a better estimate of the transfer function related to the I_{VS3} channel, while leaving the one that links z_p to V_{VS3} practically unaffected.

It is worth to observe that, in the proposed VS architecture (fig. 3), the quantities that are fed back to the controller are I_{VS3} and \dot{z}_p , so the static gain of the loop transfer function will depend only on the gain on I_{VS3} . A precise knowledge of this gain allows to exactly fix the upper gain margin of the system when designing the VS controller (see discussion in sec. 4).

4. Controller design

We are now ready to introduce a procedure to automatically design a controller in the form (12) based on the model (18). To clarify the choices made in this procedure, as a running example we will again consider the full-order and identified (including the fit of the static gain on I_{VS3}) linear models of sec. 3.3, related to the time instant $t = 2.4$ s in the ramp-down scenario of sec. 5.1.

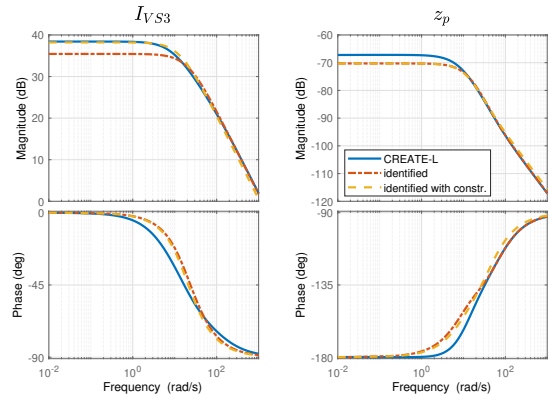


Figure 7: Comparison between the CREATE-L (solid blue) and identified linear models at $t = 2.4$ s (with and without the static gain correction, dash-dotted red and dashed yellow lines respectively). To compare the Bode diagrams, the identified model has been converted to a continuous-time one in MATLAB by using the 'zoh' method. For this example, a weight $\alpha = 400$ has been used to fit the static gain of the I_{VS3} channel.

As it was discussed in sec. 2.3, we aim at designing a controller based on the feedback of the in-vessel current I_{VS3} and of the plasma vertical velocity \dot{z}_p , where the latter is estimated by means of a derivative filter. We add this filter in series to the transfer function $P(s)$ associated to eq. (18) (see the HPF block in fig. 3)

$$G(s) = \begin{bmatrix} 1 & 0 \\ 0 & F(s) \end{bmatrix} P(s) \quad (27)$$

In the design procedure we approximate the HPF with an ideal derivative, i.e. $F(s) = s$. The resulting channels for $G(s)$ have the form

$$G_I(s) = \frac{\bar{G}_I(s - \tilde{\gamma})}{(s - \gamma)(s + \tilde{p})} \quad (28a)$$

$$G_{\dot{z}}(s) = \frac{\bar{G}_z s(s + \tilde{z})}{(s - \gamma)(s + \tilde{p})} \quad (28b)$$

with $\gamma, \tilde{\gamma}, \tilde{p}, \tilde{z} > 0$. The transfer functions $G_I(s), G_{\dot{z}}(s)$ have a positive real part pole that corresponds to the (identified) growth rate γ , and a second pole \tilde{p} that is expected to be negative and real. Moreover, note that the non-minimum phase zero $\tilde{\gamma}$ in the transfer function for the I_{VS3} channel will usually be close to the growth rate γ (in the example of sec. 3.3, $\tilde{\gamma} = 11.7$ and $\gamma = 11.08$). From a physical standpoint, this depends on the fact that the unstable mode is not easily detectable from the measurement of the in-vessel current. On

the other hand, a zero appears in the \dot{z}_p channel as well, due to the direct feedthrough of the voltage vertical velocity ($d \neq 0$ in eq. (17)).

By considering the control law (12) we obtain the following open-loop transfer function ²

$$\begin{aligned} L(s) &= K_z G_{\dot{z}}(s) + K_I G_I(s) \\ &= K_z \left(G_{\dot{z}}(s) + \frac{K_I}{K_z} G_I(s) \right) \end{aligned} \quad (29)$$

The second order polynomial at the numerator of $L(s)$ may have complex conjugate roots. To avoid a decrease of the loop gain in the neighborhood of the natural frequency of these zeros, it is important to guarantee that the damping factor is sufficiently large. Indeed, it was observed that a low damping factor decreases the attainable phase margin at the input of the plant.

Hence, in order to increase the damping factor associated to these zeros, we study the discriminant of this polynomial, which is itself a second order function of the parameter $\bar{K} := K_I/K_z$ given by

$$\Delta(\bar{K}) = \bar{G}_I^2 \bar{K}^2 - 2(\tilde{z} \bar{G}_I \bar{G}_z + 2\tilde{\gamma} \bar{G}_I \bar{G}_z) \bar{K} + \tilde{z}^2 \bar{G}_z^2. \quad (30)$$

By setting $\Delta \geq 0$ we enforce the zeros of the loop transfer function to be real. A good choice for \bar{K} then is to take the smallest root of Δ , which we denote with λ_m . By simple calculations, it can be shown that the discriminant of the 2nd order polynomial (30) is always positive for $\tilde{\gamma}, \tilde{z} > 0$, which guarantees that two real roots exist and the procedure described in this section can be applied. On the other hand, the *a posteriori* verification of this last condition can be used as a validity test for the resulting identified model.

By also explicitly taking into account the power supply model (14), eq. (29) becomes

$$L_{PS}(s) = K_z (G_{\dot{z}}(s) + \lambda_m G_I(s)) W_{PS}(s) \quad (31)$$

We then choose K_z so as to ensure an upper gain margin of at least 6 dB. If we denote the static gain of $L_{PS}(s)$ by L_0 , we can choose for example

$$K_z = -2.1/L_0$$

Notice that the static gain L_0 depends on the gain on the I_{VS3} current only, as the \dot{z}_p channel has zero

²In order to obtain a SISO transfer function to work on, we consider the open loop transfer function that links the output of the controller to the voltage request to the power supplies V_{VS3} .

static gain. As a consequence, thanks to the fitting procedure described in sec. 3.4, a quite accurate estimate of L_0 is available. It is also worth to remark that the proposed controller closes a positive feedback loop on the in-vessel current and a negative one on the plasma vertical velocity; for more details about this point, see the discussion in [26].

The procedure described so far leads, for the case under examination, to a loop function with a rather high crossing frequency ω_c of about 270 rad/s, as it can be seen from fig. 8), which may negatively interact with the actual power supplies and diagnostics. Indeed, in order to have a sufficiently small phase delay due to the actuator and diagnostics, in the design procedure the crossing frequency has been fixed to 40 rad/s. To achieve the desired value for ω_c , we introduce in the controller a lag network in the form

$$\frac{1 + i\omega \frac{\tau}{m}}{1 + i\omega\tau}$$

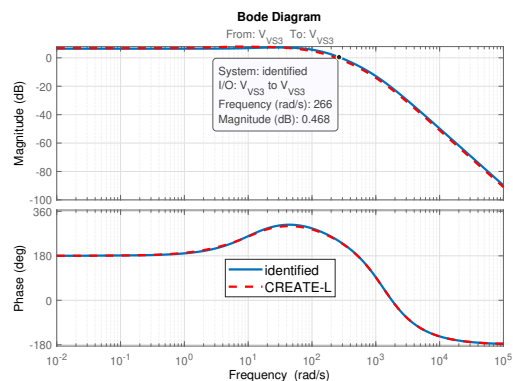


Figure 8: Bode diagram of the loop function (31) for the full-order (CREATE-L) and identified linearized models. In the plot, a 2nd order Padé approximant of the delay term has been used.

The network is parameterized in τ , the characteristic frequency of the pole, and m , which defines the pole-zero distance. In our procedure, we fix $m = 3$ and scan the values of τ in order to obtain the desired attenuation at the crossing frequency (in a practical implementation, the values of the attenuation at different values of τ can be pre-computed offline and stored in a look-up table). Note that the phase margin is quite large, as it can be seen in fig. 8, so the lag introduced by the network is acceptable.

The resulting controller is

$$R(s) = \frac{1 + s\frac{\tau}{3}}{1 + s\tau} [K_I, K_z], \quad (32)$$

$$K_z = -\frac{2.1}{L_0}, \quad K_I = -K_z \lambda_m.$$

Fig. 9 shows the Nichols chart resulting from the application of the control law (32) to the considered example. It can be seen that the loop function has a large phase margin of about 90° and upper and lower gain margins of 6.7 and 16 dB respectively.

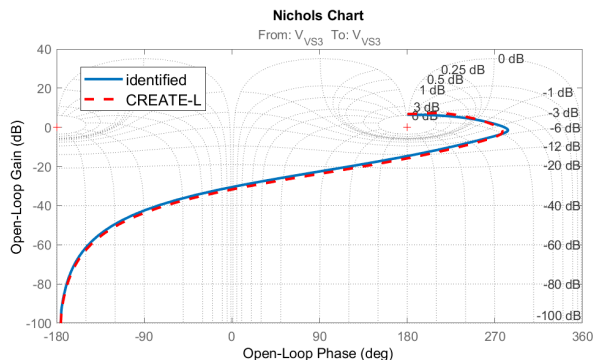


Figure 9: Nichols chart of the loop function obtained by applying the control law (32). In the plot a 2^{nd} order Padé approximant of the delay term has been used.

5. Numerical simulations

To test the effectiveness of the procedure, non-linear simulations have been carried using the CREATE-NL+ code. These simulations include a portion of ramp-down from a baseline ITER scenario and a transition between two different plasma configurations. Moreover, analyses based on a CREATE-L linearized model have been used to assess the impact of measurement noise on the considered quantities.

5.1. Plasma ramp-down

The first simulated scenario is the portion of the ITER ramp-down already described in sec. 3.3.

As it can be seen from fig. 11, the controllers that results by the proposed identification/design procedure are able to stabilize the plasma through all the considered scenario segment. In particular, the different panels show the plasma centroid vertical position (the slow drift is due to the fact that the plasma current is ramping down) and velocity, and the VS3 current and voltage, which are brought

	γ	β_p	l_i	κ	δ
Initial eq.	4.92	0.66	0.88	1.77	0.44
Final eq.	3.92	0.77	0.76	1.80	0.44

Table 1: Parameters for the initial and final plasma configurations considered in the simulation of sec. 5.2: growth rate γ , profile parameters β_p and l_i , elongation κ and triangularity δ .

close to zero at steady state. It is worth to notice that, in many magnetic control systems, the K_z gain in the control law 12 is scaled linearly with the plasma current; in the present application, however, this is not done explicitly, since the identification procedure is run frequently enough to compensate for the I_p variation.

5.2. Plasma growth rate variation

In the next simulation, we consider a different plasma configuration with a lower growth rate, which varies from ~ 5 to $\sim 4 \text{ s}^{-1}$ over a time interval of 13s. The segment is obtained by transitioning between two plasma configurations, whose parameters are shown in table 1.

The results obtained for this simulation in terms of the plasma current and the controlled quantities are shown in fig. 13, while fig. 14 shows the actual and identified growth rates. It can be seen that the algorithm identifies the value of γ with a good accuracy, even if a slight oscillation can be seen in fig. 14, probably induced by the change in direction of the VS kicks.

5.3. Effect of measurement noise

Finally, in this section we analyze the effect of an additive measurement noise on the data used in the identification procedure on the accuracy of the identified model. To do so, we chose a linearized model of the plasma response associated to a plasma configuration with a growth rate $\gamma \approx 4.9$, and we carried out the identification in the presence of different levels of measurement noise; then, we compared the resulting identified growth rates with the actual value.

In particular, for the I_{VS3} current we considered a white Gaussian noise with $\sigma_I \in [0, 10]\%$ of I_{VS3} . Notice that this value is significantly larger with respect to the foreseen ITER PF current measurement noise, for which two contributes are foreseen, one expressed in percent with respect to the current value and with a standard deviation of $\sigma = 0.1\%$, and the other with a very low fixed standard deviation

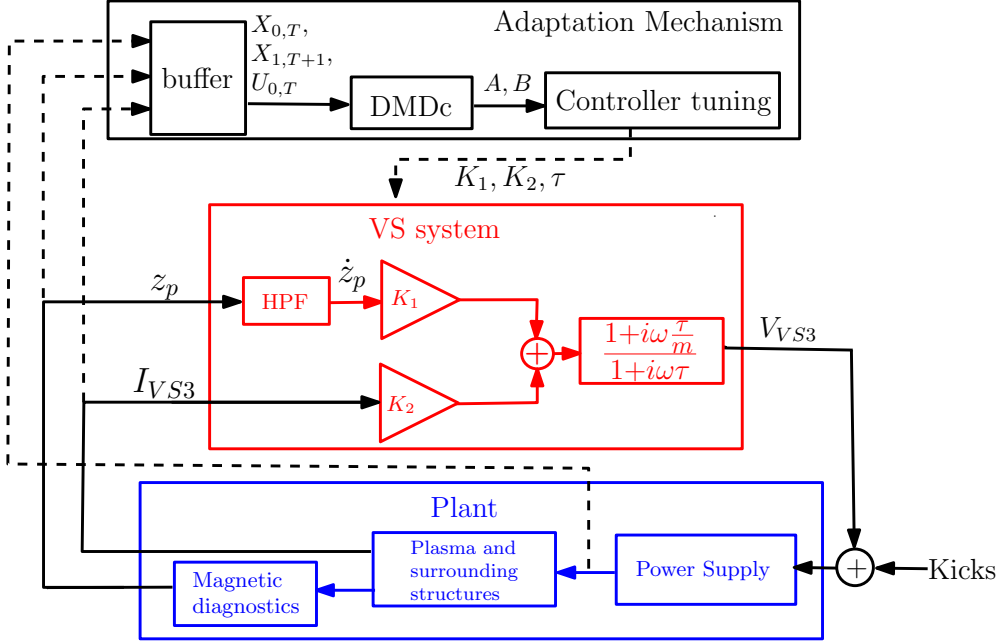


Figure 10: Resulting VS control scheme. The parameters of the VS controller (12) are adjusted by the adaptation mechanism described in sections 3 and 4, and voltage kicks are introduced in the scheme as additional inputs to the VS3 circuit.

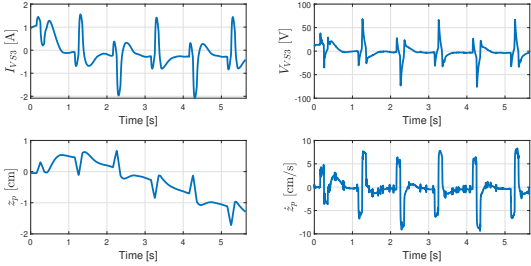


Figure 11: Ramp-down simulation: I_{VS3} current (top-left panel), V_{VS3} voltage (top-right), plasma centroid position z_p (bottom-left) and velocity \dot{z}_p (bottom-right).

$\sigma = 3.5$ A [34] (the latter term has been neglected in this analysis). For what concerns z_p instead, we considered again an additive white Gaussian noise with standard deviation $\sigma_z \in [0, 5]$ mm. It is again worth to notice that 5 mm represent a significant error on z_p , since usually maximum displacements in the order of a few centimeters are considered (see for example fig. 11). No noise has been added to the control action V_{VS3} , for which we assumed to have an accurate measurement available. In order to quantify a worst-case scenario performance, for each tile in fig. 15 we considered 5 different noise realizations and took the largest resulting error in

terms of γ fitting.

To cope with the significant level of noise introduced in the scheme, in this simulation the kicks amplitude is increased to 250 V. The maximum gap variation produced by these kicks is about 4cm, which never causes the plasma to touch the surrounding wall. Moreover, applying a smoothing filter to the data turned out to be greatly beneficial to the identification accuracy. It is worth to remark that, since all the data are collected before running the identification procedure, a non-causal smoothing filter can be employed, i.e. no delay is introduced by the filtering action. For this analysis, we used a moving average filter with a window of 70 samples.

The results in terms of accuracy of the identified model are shown in fig. 15, that shows the error in terms of the resulting model's growth rate when compared with the actual one. The four bode plots in fig. 16 refer to the cases where no noise is considered and where the maximum noise on either I_{VS3} , z_p or both signals is applied. Remarkably, the resulting controller is capable of stabilizing the plant in all these four cases, despite the very high levels of noise and the resulting fitting error in terms of γ .

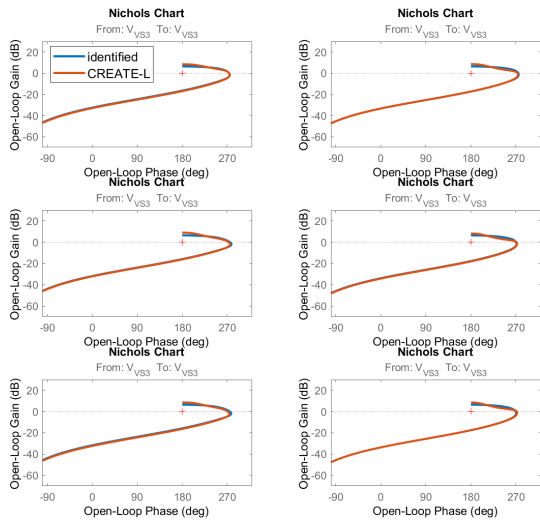


Figure 12: Nichols chart of the loop function obtained by applying the control law (32) for all the identified systems. The loop functions with both the identified (blue) and actual (red) dynamics are shown. In the plots, a 2nd order Padé approximant of the delay term has been used.

6. Conclusions

In this article, an online tuning procedure for the parameters of the VS controller of the ITER tokamak has been proposed. The identification procedure, based on the DMDc approach, periodically updates a simplified 2nd order model, that can be used online to tune/design a stabilizing controller. In this view, a possible design procedure, based on linear controller synthesis techniques, has been proposed and applied to different test cases. The procedure also includes a method to refine the estimate of the static gain by taking into account the knowledge of the stabilization circuit resistance. The proposed data-driven approach proved effective in different scenarios, and is able to cope with significant levels of measurement noise.

Currently, the main limitation of the proposed approach is that the identification procedure does not take into account variations in the internal plasma current distribution. The choice made in this work was to run the identification algorithm far from transient phases, such as LH/HL transitions, in order to avoid a degradation of the estimation accuracy due the presence of external disturbances that are not accounted for. However, modified versions of the proposed technique could be investigated, where an online knowledge of the plasma internal pro-

files (usually provided in real tokamak discharges by Magnetic/Kinetic Equilibrium Reconstruction algorithms in terms of few, synthetic descriptors) is explicitly taken into account in the model identification.

References

- [1] J. Wesson and D.J. Campbell. *Tokamaks*, volume 149. Oxford university press, 2011.
- [2] G. Ambrosino and R. Albanese. Magnetic Control of Plasma Current, Position and Shape in Tokamaks. *IEEE Contr. Sys. Mag.*, 25(5):76–92, 2005.
- [3] M. Ariola and A. Pironti. *Magnetic Control of Tokamak Plasmas*. Springer, 2nd edition, 2016.
- [4] E.A. Lazarus, J.B. Lister, and G.H. Neilson. Control of the vertical instability in tokamaks. *Nuclear Fusion*, 30(1):111, 1990.
- [5] M.L. Walker and D.A. Humphreys. On feedback stabilization of the tokamak plasma vertical instability. *Automatica*, 45(3):665–674, 2009.
- [6] F. Sartori, G. De Tommasi, and F. Piccolo. The Joint European Torus. *IEEE Contr. Sys. Mag.*, 26(2):64–78, 2006.
- [7] E. Schuster et al. Plasma vertical stabilization with actuation constraints in the DIII-D tokamak. *Automatica*, 41(7):1173–1179, 2005.
- [8] G. Ambrosino, M. Ariola, G. De Tommasi, A. Pironti, and A. Portone. Design of the plasma position and shape control in the ITER tokamak using in-vessel coils. *IEEE transactions on plasma science*, 37(7):1324–1331, 2009.
- [9] G. Ambrosino et al. Plasma Vertical Stabilization in the ITER Tokamak via Constrained Static Output Feedback. *IEEE Trans. Contr. Sys. Tech.*, 19(2):376–381, 2011.
- [10] R. Albanese, R. Ambrosino, A. Castaldo, G. De Tommasi, Z.P. Luo, A. Mele, A. Pironti, B.J. Xiao, and Q.P. Yuan. ITER-like vertical stabilization system for the EAST tokamak. *Nuclear Fusion*, 57(8):086039, 2017.
- [11] L. Scibile and B. Kouvaritakis. A discrete adaptive near-time optimum control for the plasma vertical position in a tokamak. *IEEE Trans. Contr. Sys. Tech.*, 9(1):148–162, 2001.
- [12] S. Geršković and G. De Tommasi. Vertical stabilization of ITER plasma using explicit model predictive control. *Fus. Eng. Des.*, 88(6):1082–1086, 2013.
- [13] N.N. Bao, Y. Huang, J. Barr, Z.P. Luo, Y.H. Wang, S.L. Chen, B.J. Xiao, and D. Humphreys. Tests of the real-time vertical growth rate calculation on east. *Chinese Physics B*, 29(6):065204, 2020.
- [14] G. De Tommasi, S. Dubbioso, A. Mele, and A. Pironti. Stabilizing elongated plasmas using extremum seeking: the ITER tokamak case study. In *2021 29th Mediterranean Conference on Control and Automation (MED)*, pages 472–478, 2021.
- [15] S. Dubbioso, L.E. di Grazia, G. De Tommasi, M. Mattei, A. Mele, and A. Pironti. Vertical stabilization of tokamak plasmas via extremum seeking. *IFAC Journal of Systems and Control*, 21:100203, 2022.
- [16] J.L. Proctor, S.L. Brunton, and J.N. Kutz. Dynamic mode decomposition with control. *SIAM Journal on Applied Dynamical Systems*, 15(1):142–161, 2016.

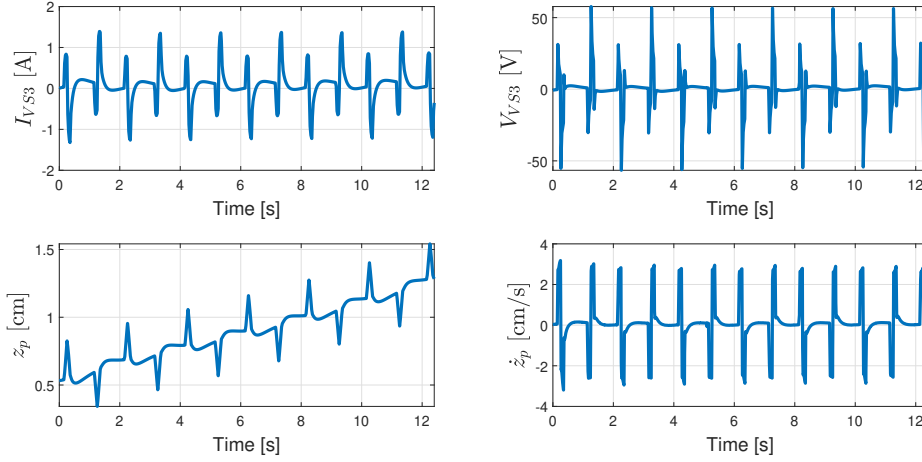


Figure 13: Simulation of a plasma shape variation: I_{VS3} current (top-left panel), V_{VS3} voltage (top-right), plasma centroid position z_p (bottom-left) and velocity \dot{z}_p (bottom-right).

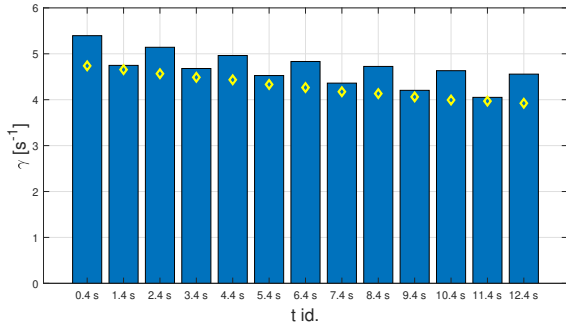


Figure 14: Growth rate (actual vs identified) for the simulation of sec. 5.2. The blue bars represent the identified eigenvalues, while the yellow diamonds are the growth rates of the resulting linearized models. The oscillating behaviour suggests that the identification is more accurate in the case of a downward-upward kick.

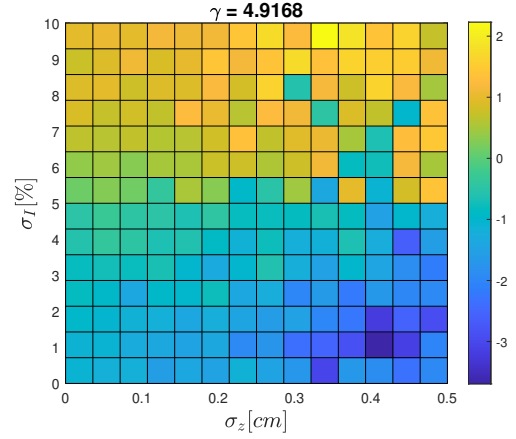


Figure 15: Identification accuracy in presence of different levels of noise, expressed in terms of the difference between the actual and the identified growth rate. The Bode plots corresponding to the four corners of this graph are shown in fig. 16.

- [17] J.N. Kutz, S.L. Brunton, Bingni W. Brunton, and J.L. Proctor. *Dynamic mode decomposition: data-driven modeling of complex systems*. SIAM, 2016.
- [18] P. J. Schmid and J. L. Sesterhenn. Dynamic mode decomposition of numerical and experimental data. In *Bull. Amer. Phys. Soc. 61st Annual Meeting of the APS Division of Fluid Dynamics, San Antonio TX*, volume 53, page 208. Amer. Phys. Soc., College Park, MD, 2008.
- [19] P.J. Schmid. Dynamic mode decomposition of numerical and experimental data. *Journal of fluid mechanics*, 656: 5–28, 2010.
- [20] C.W. Rowley, I. Mezić, S. Bagheri, P. Schlatter, and D.S. Henningson. Spectral analysis of nonlinear flows. *Journal of fluid mechanics*, 641:115–127, 2009.
- [21] R. Taylor, J N. Kutz, K. Morgan, and Brian A Nelson. Dynamic mode decomposition for plasma diagnostics and validation. *Review of Scientific Instruments*, 89(5): 053501, 2018.

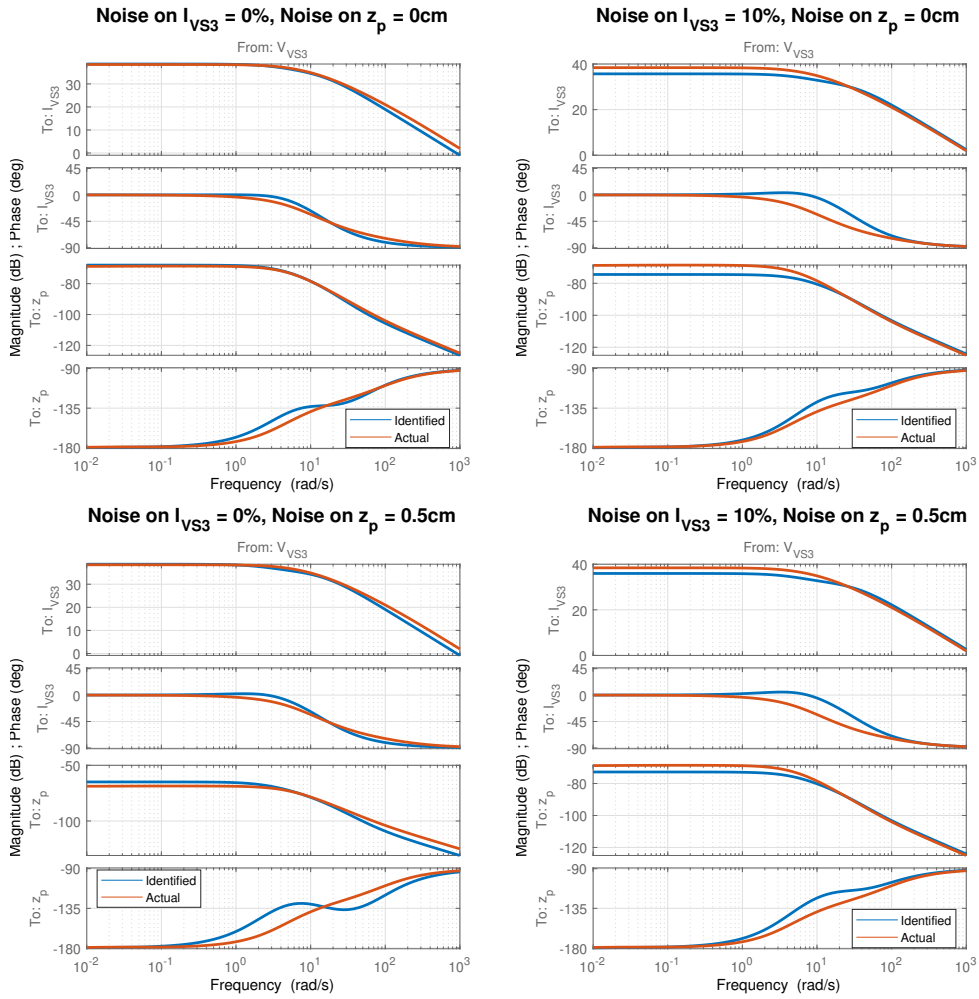


Figure 16: Examples of identified vs. actual Bode diagrams, taken from the analysis shown in fig. 15. The panels (from top-left in clockwise direction) represent the cases where no noise is applied or when the maximum level of noise is applied to I_{VS3} only, both I_{VS3} and z_p or z_p only respectively.

- [22] H. Natsume, H. Tanaka, S. Kajita, and N. Ohno. Application of dynamic mode decomposition to rotating structures in detached linear plasmas. *Physics of Plasmas*, 27(4):042301, 2020.
- [23] A.A. Kaptanoglu, K.D. Morgan, C.J. Hansen, and S.L. Brunton. Characterizing magnetized plasmas with dynamic mode decomposition. *Physics of Plasmas*, 27(3):032108, 2020.
- [24] R. Albanese, R. Ambrosino, and M. Mattei. CREATE-NL+: A robust control-oriented free boundary dynamic plasma equilibrium solver. *Fus. Eng. Des.*, 96–97:664–667, 2015.
- [25] R. Albanese and F. Villone. The linearized CREATE-L plasma response model for the control of current, position and shape in tokamaks. *Nucl. Fus.*, 38:723, 1998.
- [26] G. De Tommasi, A. Mele, Z.P. Luo, A. Pironti, and B.J. Xiao. On plasma vertical stabilization at EAST tokamak. In *2017 IEEE Conference on Control Technology and Applications (CCTA)*, pages 511–516. IEEE, 2017.
- [27] G. De Tommasi, A. Mele, and A. Pironti. Robust plasma vertical stabilization in tokamak devices via multi-objective optimization. In *Int. Conf. on Optimization and Decision Science*, pages 305–314, 2017.
- [28] E. Gaio, R. Piovan, V. Toigo, and I. Benfatto. The control system of the ITER vertical stabilization converter. *Fusion engineering and design*, 66:719–725, 2003.
- [29] R. Albanese, E. Coccoresse, and G. Rubinacci. Plasma modelling for the control of vertical instabilities in tokamaks. *Nuclear Fusion*, 29(6):1013, 1989.
- [30] D.A. Humphreys and I.H. Hutchinson. Axisymmetric magnetic control design in tokamaks using perturbed equilibrium plasma response modeling. *Fusion Technology*, 23(2):167–184, 1993.
- [31] A.S. Welander, R.D. Deranian, D.A. Humphreys, J.A. Leuer, and M.L. Walker. Nonrigid, linear plasma response model based on perturbed equilibria for axisymmetric tokamak control design. *Fusion science and technology*, 47(3):763–767, 2005.
- [32] C. De Persis and P. Tesi. Formulas for data-driven control: Stabilization, optimality, and robustness. *IEEE Transactions on Automatic Control*, 65(3):909–924, 2019.
- [33] E. de la Luna, I.T. Chapman, F. Rimini, P.J. Lomas, G. Saibene, F. Koechl, R. Sartori, S. Saarelma, R. Albanese, J. Flanagan, et al. Understanding the physics of elm pacing via vertical kicks in jet in view of iter. *Nuclear Fusion*, 56(2):026001, 2015.
- [34] Y. Huang, A. Mele, Z.P. Luo, M. Mattei, A. Pironti, B.J. Xiao, and Q.P. Yuan. Implementation of a Kalman filter-based eddy current estimator for the P-EFIT magnetic equilibrium reconstruction code. *Nuclear Fusion*, 62(8):086010, 2022.